

Inhibition of Calcium Dependent Protein Kinase 1 (CDPK1) by Pyrazolopyrimidine Analogs Decreases Establishment and Reoccurrence of Central Nervous System Disease by *Toxoplasma gondii*

Florentine U. Rutaganira,[†] Jennifer Barks,^{‡,△} Mary Savari Dhason,^{‡,△} Qiuling Wang,^{‡,△} Michael S. Lopez,^{†,§} Shaojun Long,[‡] Joshua B. Radke,[‡] Nathaniel G. Jones,[‡] Amarendar R. Maddirala,[§] James W. Janetka,[§] Majida El Bakkouri,^{||} Raymond Hui,^{||,⊥} Kevan M. Shokat,^{†,¶} and L. David Sibley^{*‡,§,¶}

[†]Howard Hughes Medical Institute and Department of Cellular and Molecular Pharmacology, University of California, San Francisco, San Francisco, California 94158, United States

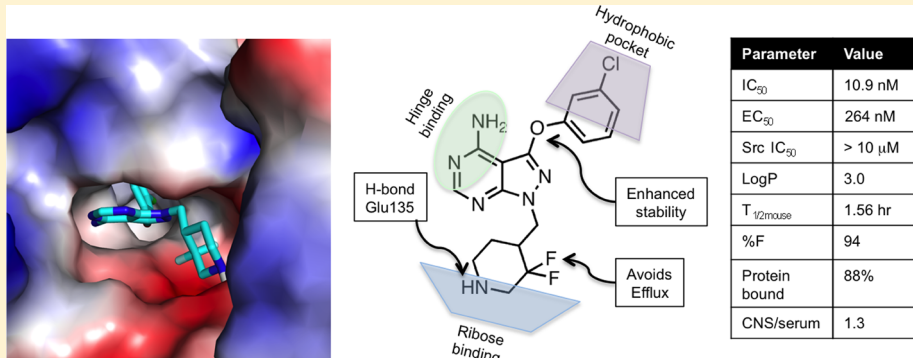
[‡]Department of Molecular Microbiology, Washington University School of Medicine, St. Louis, Missouri 63130, United States

[§]Department of Biochemistry and Molecular Biophysics, Washington University School of Medicine, St. Louis, Missouri 63130, United States

^{||}Structural Genomics Consortium, University of Toronto, MaRS South Tower, 101 College St, Toronto, ON M5G 1L7, Canada

[⊥]Toronto General Hospital Research Institute, 200 Elizabeth St., Toronto, ON M5G 2C4, Canada

Supporting Information



ABSTRACT: Calcium dependent protein kinase 1 (CDPK1) is an essential enzyme in the opportunistic pathogen *Toxoplasma gondii*. CDPK1 controls multiple processes that are critical to the intracellular replicative cycle of *T. gondii* including secretion of adhesins, motility, invasion, and egress. Remarkably, CDPK1 contains a small glycine gatekeeper residue in the ATP binding pocket making it sensitive to ATP-competitive inhibitors with bulky substituents that complement this expanded binding pocket. Here we explored structure–activity relationships of a series of pyrazolopyrimidine inhibitors of CDPK1 with the goal of increasing selectivity over host enzymes, improving antiparasite potency, and improving metabolic stability. The resulting lead compound **24** exhibited excellent enzyme inhibition and selectivity for CDPK1 and potently inhibited parasite growth in vitro. Compound **24** was also effective at treating acute toxoplasmosis in the mouse, reducing dissemination to the central nervous system, and decreasing reactivation of chronic infection in severely immunocompromised mice. These findings provide proof of concept for the development of small molecule inhibitors of CDPK1 for treatment of CNS toxoplasmosis.

INTRODUCTION

Toxoplasma gondii is a widespread protozoan parasite of animals that causes zoonotic infections in humans. Although most human cases are well controlled, infection in immunocompromised patients leads to serious sequelae, including toxoplasmic encephalitis and pneumonia, which are life-threatening if not treated.¹ Although the advent of HAART therapy has reduced the frequency of toxoplasmosis as an opportunistic pathogen in developed countries, it is still a serious complication in many parts of the world where

patients do not have adequate access to testing or treatment for HIV infection.^{2–5} Additionally, toxoplasmosis can cause serious problems in organ transplant and cancer chemotherapy patients due to their immunocompromised status.⁶ Furthermore, toxoplasmosis is a recognized cause of severe ocular disease in healthy adults in some locations such as Brazil.⁷

Received: August 14, 2017

Published: September 21, 2017

Current therapy for toxoplasmosis is based on combination of pyrimethamine, which blocks dihydrofolate reductase (DHFR), and sulfadiazine, a folate antagonist. Collectively these drugs disrupt replication by inhibiting nucleic acid synthesis. This drug combination is efficacious in treating acute infection through blocking replication of tachyzoites. Unfortunately pyrimethamine is associated with several adverse side effects including anemia due to bone marrow suppression,⁸ and many patients experience allergic reactions to sulfonamide drugs.⁹ Chronic infections caused by *T. gondii* are typified by slow growing bradyzoites that reside within thick-walled tissue cysts.¹⁰ The emergence of bradyzoites upon cyst rupture is thought to give rise to daughter cysts that sustain the chronic infection and contribute to recurrence of actively replicating tachyzoites when the parasite reverts to the lytic form. Hence, treatments that could block re-emergence from the tissue cyst or block invasion of host cells by bradyzoites could interrupt this cycle and eliminate chronic infection. Unfortunately, current therapies that inhibit DHFR and antagonize the folate pathway are not effective at clearing chronic infection, as evidenced by the high relapse in immunocompromised patients when therapy is discontinued,⁹ presumably due to the slow and sporadic replication of bradyzoites.

One of the key steps in defining new leads for therapeutic intervention is to identify essential pathways that can be targeted by small molecules. One potential new target that fulfills these criteria is calcium dependent protein kinase 1 (CDPK1) in *T. gondii*.¹² Genetic depletion or chemical inhibition of CDPK1 blocks adhesion secretion and compromises motility, cell invasion, and egress,¹² thus demonstrating the essentiality of this target. The X-ray crystal structure of CDPK1 also revealed an unusual feature in the ATP-binding pocket where a glycine residue occupies the gatekeeper position where there is normally a larger hydrophobic residue.^{13,14} The presence of G gatekeeper is entirely unprecedented in human kinases,¹⁵ and CDPK1 is the only kinase in *T. gondii* with this unusual feature.¹⁶ As a consequence, CDPK1 is exquisitely sensitive to bulky ATP competitive inhibitors such as pyrazolopyrimidines (PP), which mimic the nucleotide binding interactions with the hinge region within the ATP-binding pocket and project bulky substituents into the expanded hydrophobic pocket created by the G gatekeeper.^{17,18} These features have been exploited to develop PP analogs that are potent inhibitors of CDPK1 in *T. gondii*,^{19–21} and the most promising of these compounds show good efficacy in mouse models of toxoplasmosis.^{22–24}

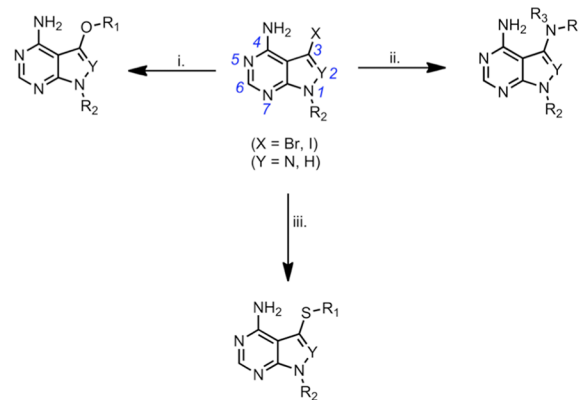
Our prior studies involving derivatives with substituents (R_1) to the C3 position of the pyrazolopyrimidine (PP) core revealed the importance of the methylene linkage at C3 to confer flexibility of R_1 substituent binding.²³ However, compounds with the methylene linkage overall were not stable in the presence of rat liver microsomes, potentially due to the methylene bridge being subject to cytochrome P450 metabolism. To address these deficiencies, we have more fully explored the design and synthesis of different heteroatom linkages at the C3 position and expanded the diversity of substituents at the R_2 position. Collectively, these rationally driven modifications have identified new TgCDPK1 inhibitors with excellent potency in addition to improved selectivity, metabolic stability, and in vivo efficacy in controlling toxoplasmosis in the mouse.

RESULTS

Design and Synthesis of New PP Analogs Targeting CDPK1. To identify compounds with improved metabolic stability that would also exploit structural differences between

CDPK1 and human Src (hSrc) active sites, we designed and synthesized a compound library containing varied functional groups at R_1 attached to the C3 position of the PP core (Scheme 1).

Scheme 1^a



^a(i) R_1OH , copper iodide, N,N -dimethylglycine, Cs_2CO_3 , dioxane, 120 °C, 18 h; (ii) R_1NH_2 , BrettPhosPd G3, $KOTBu$, dioxane, 90 °C, 18 h; (iii) R_1SH , copper iodide, ethylene glycol, 2-propanol, K_2CO_3 , 130 °C, 1 h. Positions on the PP scaffold are labeled numerically in blue italics.

These were either linked to the core pyrazolopyrimidine or pyrrolopyrimidine scaffold via methylene or heteroatom linkages (X) in combination with *t*-butyl or various R_2 groups at the N1 position (Scheme 1). The hSrc kinase was chosen for initial counter-screening because it contains a threonine (T) gatekeeper residue that represents one of the smallest amino acids found in native human kinases.¹⁵ All compounds were synthesized using previously described methods to form the pyrazolopyrimidine scaffold or with advanced pyrrolopyrimidine intermediates.^{25,26} Methods to generate compounds with methylene linkage at C3 have been previously reported,²³ and heteroatom linkages were incorporated using established aryl coupling chemistry^{27–30} (Scheme 1). Detailed procedures for chemical synthesis and compound characterization are presented in the Supporting Information.

Analysis of New PP Analogs Modified at the R_1 Position. To develop a structure–activity relationship (SAR) profile, we investigated the effects of modifying the R_1 group and different linkers to the core scaffold at position C3 in a series of compounds that contained *tertiary* butyl at the N1 position (Figure 1A). We tested compounds for their potency against CDPK1 *in vitro*, using an ELISA assay for phosphorylated substrate, described previously.²³ In parallel, we tested the inhibitors for their ability to inhibit parasite growth *in vitro* using a β -Gal expressing line of *T. gondii* to determine EC₅₀ values, as described previously.²³ Finally, we screened each analog for stability *in vitro* in the presence of rat liver microsomes, as a surrogate for estimating *in vivo* metabolic stability.

Starting with parent compound 1, replacement of the C3 methylene linker with an ether, thioether, or amine linkage improved metabolic stability for ether and amine linkages (Figure 1A). This result confirms XenoSite *in silico* predictions of metabolism at the methylene as in compound 1, which is less likely with ether and amine linkages as in compounds 2 and 4 but is still possible with thioether linkages as in 3 (Supplementary Figure S1).³¹ The thioether linkage was also associated with substantial loss of activity in the parasite inhibition assay (Figure 1A). We also observed increased metabolic stability of the ether linkage over methylene for another compound set consisting of

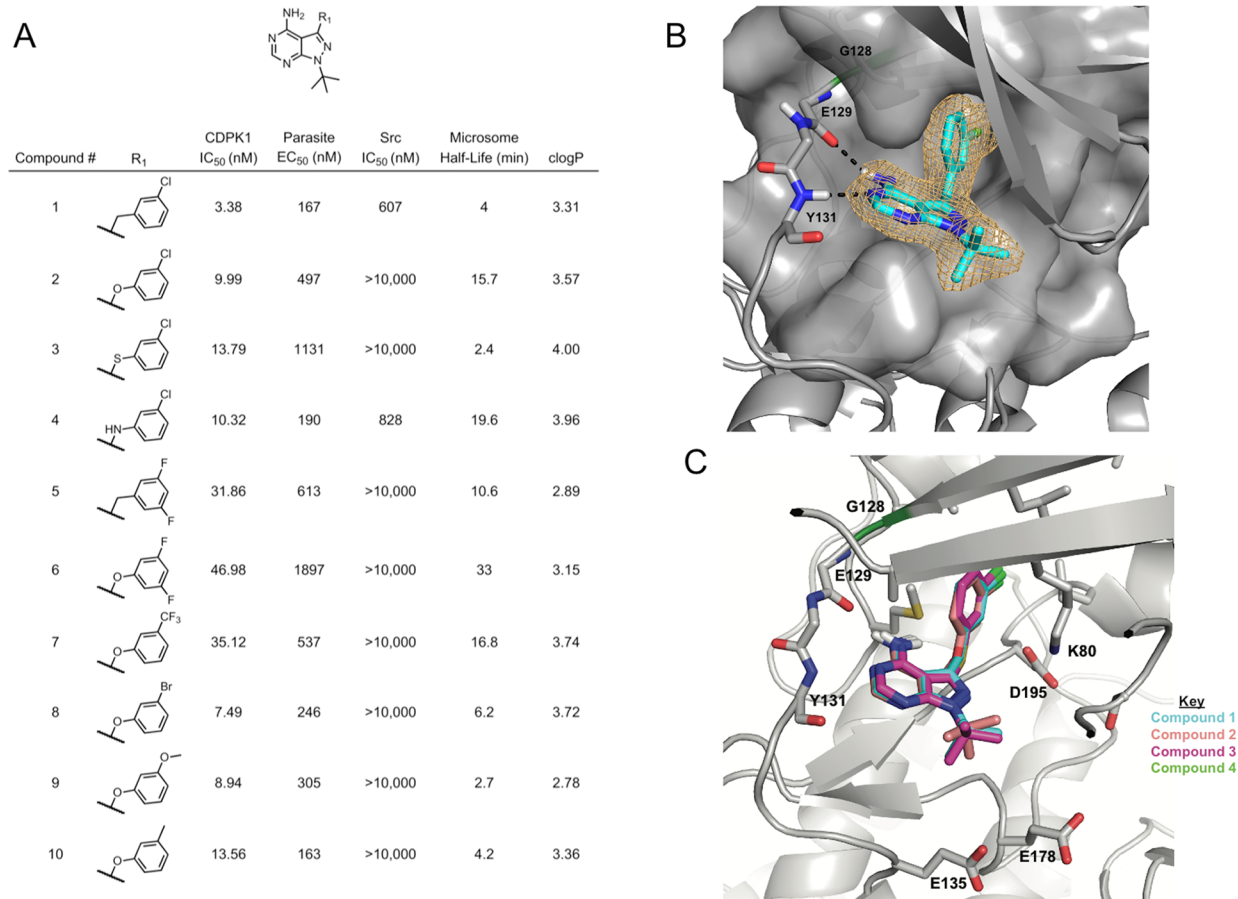


Figure 1. Structure–activity profile of initial CDPK1 inhibitor series. (A) Structures of initial CDPK1 inhibitors highlighting modifications at R₁ and heteroatom linkages of R₁ to the pyrazolopyrimidine core are shown in tabular form with associated biochemical inhibition (IC₅₀) of CDPK1, inhibition of parasite growth (EC₅₀), off-target biochemical inhibition (IC₅₀) of Src, metabolic stability in rat microsomes (half-life in minutes), and calculated clogP values. IC₅₀ and EC₅₀ values are the average of 2 or more biological replicates. (B) Compound 1 binds within the CDPK1 active site forming hydrogen bonds (black dashes) to the CDPK1 hinge and extends its R₁ substituent into the CDPK1 hydrophobic pocket. Amino acids in close proximity to compound 1 are labeled as well as the glycine gatekeeper (green). The orange map shows the 2F₀ – F_c simulated annealing map of compound 1 contoured at 1σ. (C) An overlay of compounds 1, 2, 3, and 4 shows similar binding poses for inhibitors possessing heteroatom linkages. Interacting residues are labeled as well as methionine 112 (yellow).

compounds 5 and 6. Analogs bearing halogen substitutions were generally more stable, especially in the presence of the ether linkage. The addition of some *meta* substituents on the benzyl ring was associated with loss of metabolic stability, despite having an ether linkage, for example, addition of the methoxy group in compound 9 and the methyl group for compound 10 (Figure 1A). Since the ether linkage generally improved metabolic stability while maintaining efficacy against parasite replication, we selected ether linkages for further optimization.

Structural Interactions between PP Compounds and CDPK1. To better understand the binding interactions of PP analogs and the CDPK1 enzyme, we solved a series of high-resolution cocrystal X-ray structures, using previously described methods.¹⁴ The cocrystal structure of CDPK1 with the lead compound 1 revealed a characteristic hydrogen-bonding (H-bonding) pattern of interaction between the aminopyridine and the kinase hinge. More specifically, the primary amine at C4 of the PP core acts as a H-bond donor in an interaction with the backbone carbonyl of glutamate 129, and the N5 in the PP core acts as a H-bond acceptor in an interaction with the backbone amide of tyrosine 131 (Figure 1B). Importantly, the cocrystal structures of compounds 1–4 bound to CDPK1 show that these modifications do not substantially change the binding

conformations (Figure 1C). Key H-bonding interactions between the PP core and the hinge region are maintained with R₁ occupying the hydrophobic pocket formed by the presence of the small G gatekeeper residue (Figure 1C).

Analysis of New PP Analogs Modified at the R₂ Position. Previous studies of PP analogs have shown that larger substituents are tolerated at the R₂ position and can lead to gain of potency and selectivity for CDPK1.²¹ To explore the size tolerance within the CDPK1 pocket at this region, we generated a series of analogs with cyclic amines at R₂ (Figure 2A). Structural studies have shown that methylpiperidine in the R₂ is positioned to form a H-bond with glutamate 135 in the ribose binding region of the ATP pocket of CDPK1.^{19,20} A cocrystal structure of compound 13 confirmed that this interaction is also present in the series studied here (Figure 2B). The piperidine is predicted to be protonated under physiological conditions, and as shown in the cocrystal structure, the additional H likely forms a salt bridge with glutamine 135 (Figure 2B). We explored a series of cyclic amines based on piperidine where we elucidated the importance of proper placement and direction of the amine to form the favorable charge–charge salt bridge interaction with E135. We found that any deviation from the piperidine of 13 in this series abrogated CDPK1 activity and decreased inhibition of

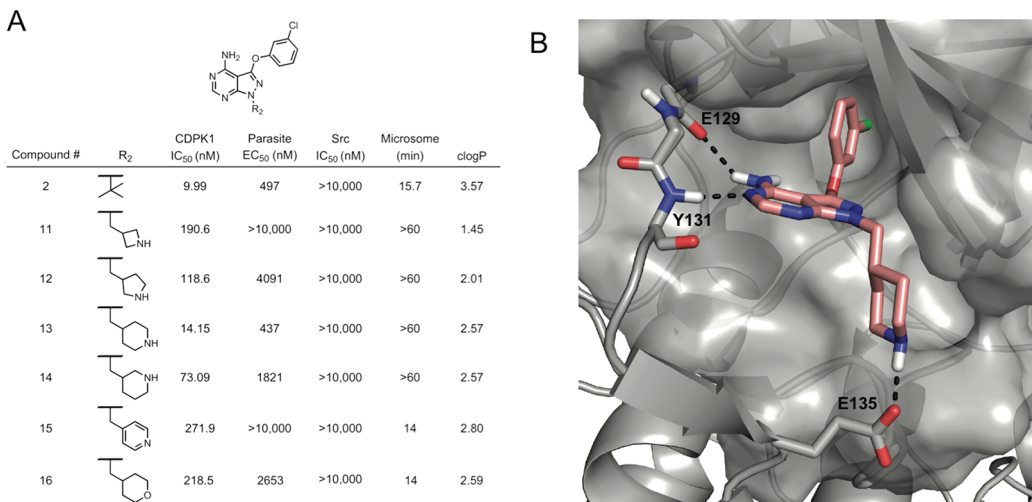


Figure 2. Exploration of R₂ with ether linked substituent. (A) Structures of CDPK1 inhibitors highlighting modifications at R₂ with *meta* chloro and ether linkage to the pyrazolopyrimidine core are shown in tabular form with associated biochemical inhibition (IC₅₀) of CDPK1, inhibition of parasite growth (EC₅₀), off-target biochemical inhibition (IC₅₀) of Src, metabolic stability in rat microsomes (half-life in minutes), and calculated clogP values. IC₅₀ and EC₅₀ values are the average of 2 or more biological replicates. (B) Compound 13 binds within the CDPK1 active site maintaining hinge binding to the CDPK1 hinge and forms an additional hydrogen bond with E135 within the CDPK1 ribose binding region.

parasite replication in culture (Figure 2A). Compounds 16 and 15, which contain a tetrahydropyran and pyridine group, respectively, each significantly lost potency, emphasizing the key contribution of the H-bond donor of the piperidine (Figure 2A). On the other hand, all cyclic amines showed greatly enhanced stability in the rat liver microsome assay thus providing much support for further R₂ modification as an approach to improving metabolic stability (Figure 2A).

In another series, we explored the combination of methylpiperidine at R₂ together with the prior functional groups at R₁ (Figure 3A). Consistent with findings above, the methylpiperidine containing analogs generally showed improved metabolic stability in comparison to their *t*-butyl counterparts (Figure 1A, 3A). For example, the presence of the methylpiperidine in compound 17 could impart stability despite having a methylene linkage to C3 of the PP core (Figure 3A). Compounds with additional halogens in the benzyl ring at R₁ gained further increases in microsome stability (e.g., 21 and 22) (Figure 3A). Furthermore, there were no significant differences between pyrazolopyrimidine and pyrrolopyrimidine as the core scaffold as demonstrated by compounds 18 vs 23 (Figure 3A).

Despite the reproducible ability of methylpiperidine to improve microsome stability throughout the entire series, this modification also resulted in reduced biochemical potency and ability to block parasite replication. Hence, incorporation of methylpiperidine at R₂ results in a trade-off between improved metabolic stability and loss in potency. This effect may be explained by the larger size of these inhibitors, which may not be as easily accommodated in the CDPK binding pocket. The combination of ether linked R₁ as *m*-Cl with R₂ piperidine as in compound 13 showed the largest improvement over parent compound 1, while retaining reasonable activity in both inhibition of CDPK1 and parasite growth (Figure 3A). In contrast, methylation of the piperidine nitrogen in compound 25 led to a loss in potency, further highlighting the importance of the H-bonding ability of the protonated amine (Figure 3A). Converting the piperidine to a 6-membered ring δ-lactam in compound 26 also lead to a loss in enzyme potency and a complete loss in antiparasitic activity (Figure 3A). We also explored modifying the piperidine by addition of difluorine (di-F), as such

modifications are known to favorably affect the properties of drug-like molecules.³² The di-F modification in compound 24 vs 13, which both have ether-linked R₁ substitutions to the PP core, slightly improved enzyme inhibition and antiparasitic activity (Figure 3A). A homology model of 24, based on the cocrystal structure of compound 13 with CDPK1, suggests that the piperidine amine is still in an appropriate position to interact with E135 (Figure 3B, Table 1). We also made a similar modification of di-F in the piperidine of compound 18 to generate the compound 28, both of which have a thioether linkage connecting R₁ to C3 in the PP core. Surprisingly in this case, the di-F modification reduced enzyme activity and greatly diminished antiparasitic activity. Modification of R₂ to contain a trifluormethylcyclopropyl moiety was also synthesized in an attempt to reduce metabolic instability, based on a previous study showing this modification can improve stability of biaryl compounds relative to those containing *t*-butyl.³³ This compound 27 lost potency (Figure 3), suggesting it does not optimally fit in the CDPK1 ATP binding pocket; moreover it did not improve stability, perhaps due to the methylene linkage of the trifluormethylcyclopropyl moiety to N1 of the core.

Inhibition of CDPK1 in Vitro Correlates with Parasite Growth Inhibition. To compare the potency of all of the new PP analogs synthesized here, we plotted the log₁₀ values for CDPK1 enzyme inhibition (IC₅₀) vs log₁₀ values for parasite growth inhibition (EC₅₀) (Figure 4A). Fitting these data with a linear regression analysis indicated a reasonable correlation (*r*² = 0.58), supporting the conclusion that the activity of these compounds against parasite growth stems largely from inhibition of CDPK1. However, the fact that this correlation is not higher suggests that *in vivo* potency is also affected by other factors. Some inhibitors lie above the diagonal line, which represents a perfect correlation, indicating they are less potent in blocking parasite growth, perhaps due to differences in cell permeability or efflux (Figure 4A). Among the most potent inhibitors was the initial lead 1, and derivatives that contain an oxygen linkage at R₁ (e.g., 2 and 10), as well as those that contain the methylpiperidine at R₂ (e.g., 13, 24) (Figure 4A). Based on a combination of potency, selectivity, and PK properties, we prioritized compounds and selected these five analogs for further study. Other compounds

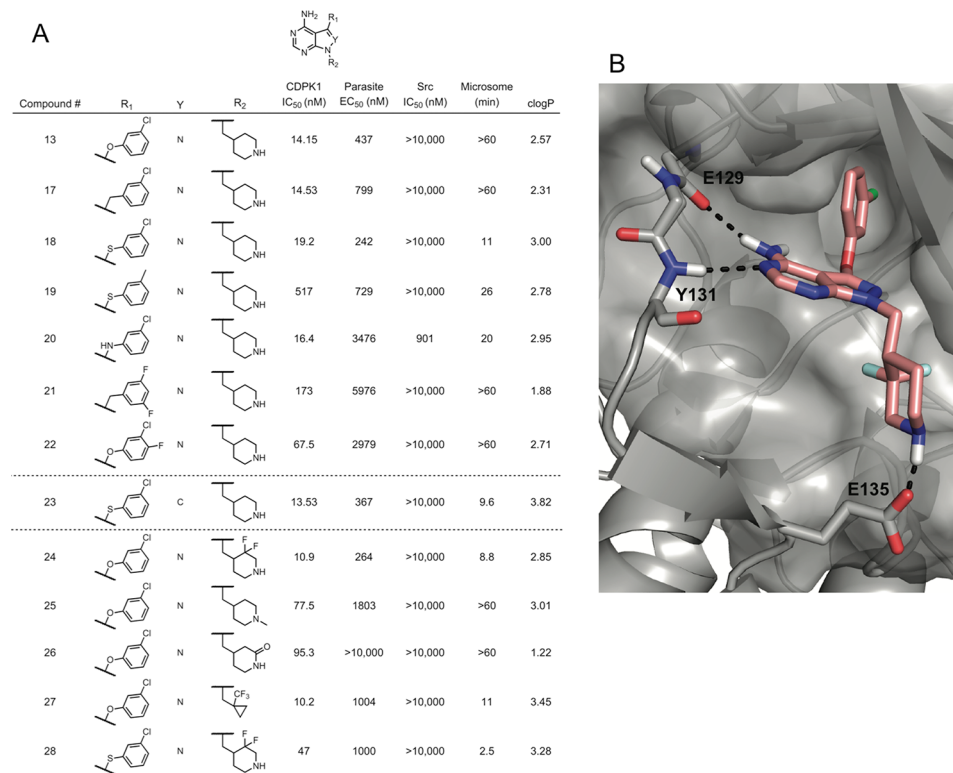


Figure 3. Exploration of methylpiperidine at R₂ for enhanced metabolic stability. (A) Structures of CDPK1 inhibitors highlighting modifications at R₁ with methylpiperidine at R₂ of a pyrazolopyrimidine core are shown in the top section, while modification of one compound to contain a pyrrolopyrimidine core that was generated in attempts to reduce cellular efflux are shown in the bottom section of the table. Biochemical inhibition (IC₅₀) of CDPK1, inhibition of parasite growth (EC₅₀), off-target biochemical inhibition (IC₅₀) of Src, metabolic stability in rat microsomes (half-life in minutes), and calculated clogP values. IC₅₀ and EC₅₀ values are the average of 2 or more biological replicates assays. (B) Homology model of compound 24 based on the cocrystal structure of compound 13 and CDPK1.

Table 1. Physical Parameters, Metabolic Stability, Efflux, And Toxicity of Select Compounds

cmpd	ClogP ^a	tPSA	pK _a	protein binding (%)	P _{app} 10 ⁻⁶ cs/s A to B ^b	P _{app} 10 ⁻⁶ cs/s B to A ^c	efflux ratio ^d	microsomes ^f CL _{int} ^e mL/(min·mg)	cell toxicity ^g (mM)
1	3.15	66.34		99.2	42.9	28.7	0.7	0.452	>10
2	3.48	75.57		99.8	34.8	30.6	0.9	0.281	>10
10	3.41	75.57		98.4	15.0	14.6	1.0	1.240	>10
13	2.57	87.6	10.4	73.5	1.07	9.58	8.9	0.019	>10
24	3.0	87.6	7.1	88.3	22.8	21.2	0.9	0.694	>10
18	3.25	78.37	10.4	87.5	2.76	25.6	9	0.072	>10
28	3.57	78.37	7.1	91.8	27.1	25.3	0.9	0.887	>10

^aDetermined in Chemdraw Ultra 12.0, PerkinElmer Informatics. ^bApparent permeability (Papp), apical to basolateral (A-B). ^cApparent permeability (Papp) basolateral to apical (B-A). ^dPapp (B to A)/Papp (A to B). ^eCL_{int} = k/P, where k is the elimination rate constant and P is the protein concentration in the assay. ^fMouse liver microsomes. ^gInhibition of replication of human HFF cells

that were potent in both assays were deprioritized for lack of specificity (e.g., 4) or lack of stability (e.g., 9).

Metabolic Stability and Cellular Update of PP Analogs.

To help choose PP analogs most likely to be active in vivo, we broadly examined the physical properties, metabolic stability in mouse liver microsomes, and cellular uptake of a select group of PP analogs (Table 1). All compounds have modest cLogP values, consistent with their intermediate hydrophobicity, and are predicted to have relatively small total polar surface area, properties that should facilitate penetration of the CNS (Table 1). Consistent with the findings in rat liver microsomes, the ether linkage in compound 2 reduced metabolic clearance in mouse liver microsomes when compared to compound 1, although both values are still relatively high (Table 1). Compound 10, which

had similar clearance to compound 1 in rat liver microsomes despite having an ether linkage, was more rapidly cleared in mouse liver microsomes (Table 1), suggesting the methyl group at C3 might be prone to metabolism. Stability was further improved when the R₂ group was switched from t-butyl to methylpiperidine as in compounds 13 and 18. However, these latter two compounds, which contain a basic amine group that is charged at neutral pH, were also associated with substantial efflux in MDCK cells (Table 1). In addition to the many other useful aspects of fluorine substitutions in medicinal chemistry, in some contexts it has been shown to reduce the basicity of proximal amines by lowering the pK_a.³⁴ Accordingly, we modified the piperidine ring by addition of difluorine (di-F), a modification that reduced the pK_a and nicely eliminated the efflux problem

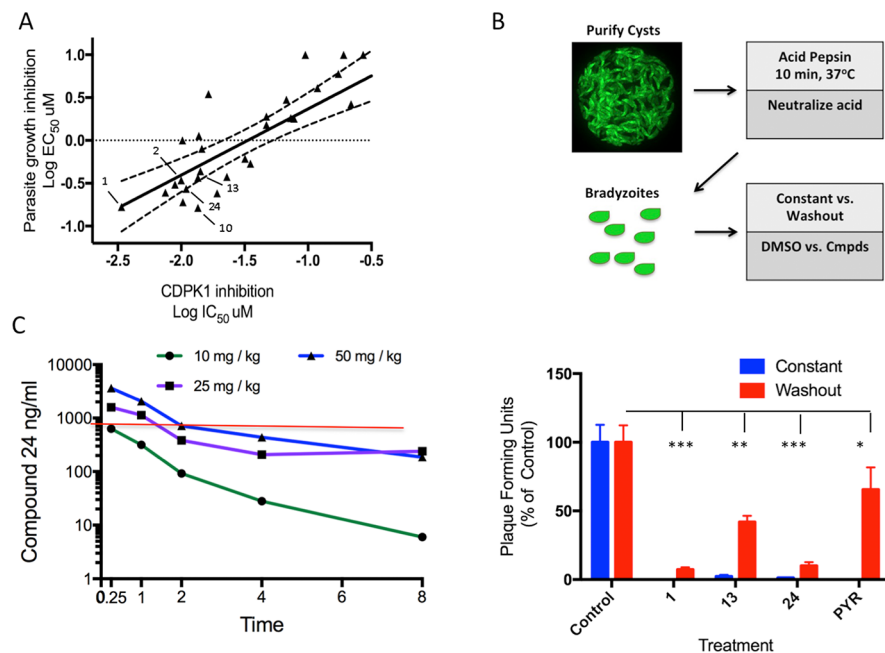


Figure 4. Activity of PP analogs against tachyzoites and bradyzoites and PK studies in mice. (A) Comparison of enzyme inhibition vs parasite growth inhibition by PP analogs. Values for IC₅₀ for inhibition of CDPK1 enzyme activity were plotted vs EC₅₀ values for inhibition of parasite growth. The plot was analyzed by linear regression (solid line), shown with 95% confidence interval (dotted lines), $r^2 = 0.58$. Highlighted are potent inhibitors that were further profiled in the following studies. (B) Ex vivo treatment of bradyzoites with PP analogs. (top) Schematic for isolation of tissue cysts containing bradyzoites, shown for PRU-GFP strain. Following Percoll enrichment of mouse-brain derived cysts, bradyzoites were liberated by acid-pepsin treatment, followed by neutralization. Liberated bradyzoites were used to infect HFF monolayers. Compounds were used to treat parallel cultures either with continuous treatment or following 4 h treatment and washing to remove extracellular parasites and compounds. (bottom) Following isolation of bradyzoites from the ME49Δhx::FLUC line, compounds were used to treat cultures as described in top panel. Plaque forming units were enumerated in triplicate from three independent experiments. Compounds 1, 13, and 24 were used at 2.5 μ M, while pyrimethamine (Pyr) was used at 3 μ M. Mean \pm SEM, $n = 3$ independent biological replicates with three technical replicates each. Two-way ANOVA with Dunnett's correction: * $P \leq 0.05$; ** $P \leq 0.01$, *** $P \leq 0.001$. (C) Pharmacokinetic analysis of compound FUR7-27 in mice. Dose dependent kinetics of serum levels of compound following oral administration. Compound 24 suspended in 25%-PEG-400-PBS with 5% DMSO was administered by oral gavage; $n = 3$ animals per time point. Reference lines shows the free serum level of compound 24 that would correspond to the EC₅₀.

(24 and 28; Table 1). However, metabolic stability was diminished by the di-F modification in these compounds. Analogs such as 1 showed high levels of plasma protein binding (PPB) (i.e., 99%); however this property was greatly reduced for compounds containing methylpiperidine or the di-F methylpiperidine (Table 1). Importantly, none of the PP analogs tested affected the growth of human foreskin fibroblasts (HFF) cells in vitro at 10 μ M, indicating that they are not toxic to host cells (Table 1).

Analysis of Target Specificity of Select PP Analogs.

To provide an assay for inhibitor selectivity, we cloned a variant of human Src, which has a threonine residue at the gatekeeper (c-Src allele), which provides for an intermediate level of sensitivity to pyrazolopyrimidine compounds.¹⁸ Although the initial lead compound 1 potently inhibited hSrc, modification of the R₁ linkage to the PP core via an ether or thioether at C3 led to greater selectivity (Figure 1A). Modification of R₂ to include cyclic amines, including piperidine, also led to large increases in selectivity for CDPK1 over hSrc (Figure 2A). Although Src has been used as a surrogate for human kinases with intermediate sensitivity to PP analogs,^{19,21} it is only one member of a diverse family of tyrosine kinases that differ substantially in their sensitivity to PP inhibitors.³⁵ As such, we profiled select inhibitors 1, 2, 13, and 24, which marked key transitions in our SAR profile. We screened all four analogs at 1 μ M against a broad panel of 489 wild type and disease-associated human kinases (Figure 5). Inhibitor selectivity increased along our SAR profile, starting from thirty-nine kinases that are inhibited or displaced by

compound 1 by over 50% to only one kinase (CK1 ϵ) that was inhibited or displaced by 24 by over 50% (Figure 5, Supplementary Table S2). Although compounds 13 and 24 exhibited IC₅₀ values of \leq 100 nM at 2 μ M ATP, these values were increased almost 10-fold in the presence of 100 μ M ATP (Supplementary Table S2). Additionally, we profiled an earlier inhibitor 3-methyl-benzyl-PP (compound 1 in ref 23) to compare our initial lead 1 in this prior series. We determined that the selectivity profile for both of these compounds was similar (Supplementary Figure S3), while selectivity was greatly increased for compounds 13 and 14. Full inhibitor profiling data is provided in the Supporting Information (Supplementary Tables S3–S5).

Potency of Select PP Analogs against ex Vivo

Bradyzoites. Previous studies have emphasized the ability of PP analogs to block host cell invasion and egress by the rapidly growing tachyzoite stage of *T. gondii*.^{19,21,23} To examine the ability of our PP inhibitors to block invasion of bradyzoites, we purified mature tissue cysts from the brains of chronically infected mice and treated them in vitro with selected PP inhibitors. We compared the effects of treatment for short intervals (i.e., 4 h followed by wash-out and further culture in the absence of compound) vs continuous treatment during a 10–14 day plaquing assay. Consistent with previous reports showing that treatment with pyrimethamine requires overnight treatment to be effective in blocking tachyzoite growth³⁶ we observed that short-term treatment with pyrimethamine had minimal effect on infection by bradyzoites, while continuous treatment blocked

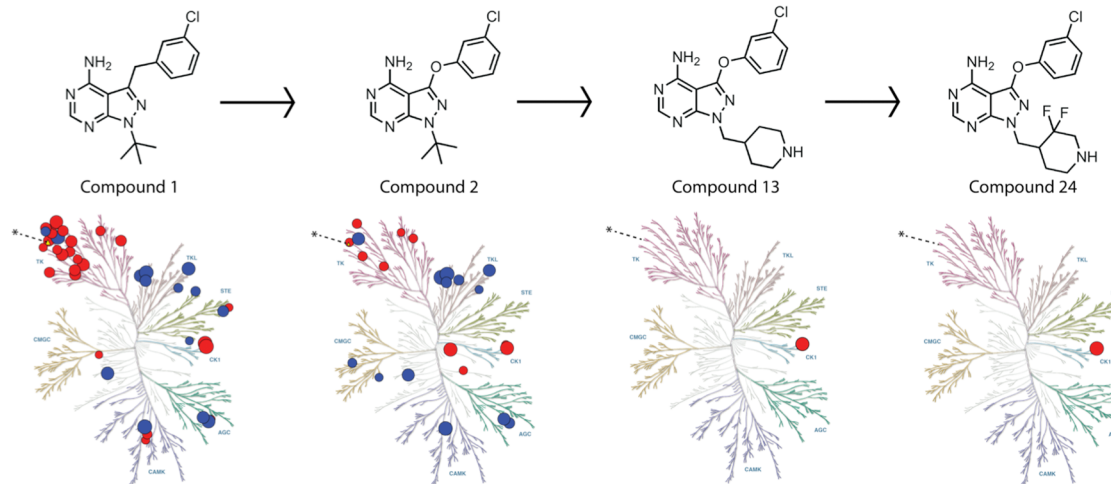


Figure 5. Human kinase profiling of compounds to determine inhibitor selectivity. Selectivity of compounds toward a panel of kinases in the ThermoFisher ACCESS program that are inhibited (red) by more than 50% or show greater than 50% tracer displacement (blue). Circle size reflects percent inhibition or displacement in the presence of inhibitor, and percentages are the mean of 2 data points. The % inhibition value for Src is shown as a yellow triangle and is emphasized by a dashed line connecting an * to the yellow triangle. Kinome tree images were generated using KinMap⁵¹ and the kinase tree illustration is reproduced courtesy of Cell Signaling Technology, Inc. (www.cellsignal.com). Inhibitors were screened at 1 μ M.

Table 2. In Vivo Pharmacokinetic Properties Based on Plasma Levels of Select Compounds

cmpd	route	dose, mg/kg	T _{max} , h	C ₀ /C _{max} ^a	ng/mL	AUC _{last} , ng/(mL h)	AUC _{inf} , ng/(mL h)	T _{1/2} , h	CL, ^b mL/(min·kg)	V _{ss} ^c , L/kg	%F ^d
1	iv	3		6892.94		1075.29	1081.76	2.06	46.22	1.09	
	po	10	0.25	585.42		918.80	930.88				26
2	iv	3		5471.09		1146.49	1149.99	1.56	43.48	1.10	
	po	10	0.25	1136.36		1172.75	1279.20				31
10	iv	3		2741.80		619.33	625.04	1.74	80	2.32	
	po	10	0.25	76.69		85.47	91.42				4
13	iv	3		535.79		449.57	523.99	3.68	95.42	19.59	
	po	10	2.00	182.56		757.85	891.24				51
24	iv	3		1205.19		975.90	988.58	1.56	50.58	3.68	
	po	10	0.25	1048.80		3058.44	3547.95				94

^aC_{max} for po route, C₀ (initial concn). ^bCL, clearance. ^cV_{ss} steady-state volume of distribution. ^dOral availability determined from AUC_{last}.

plaque formation (Figure 4B). In contrast, the PP inhibitors showed good (e.g., 13), or excellent (e.g., 1, 24), ability to block infection following even short-term incubation (Figure 4B). Because the compounds were only present during the initial interaction of the parasite with the host cell monolayer, we interpret these results to indicate that PP inhibitors can block bradyzoite entry into host cells during the 4 h treatment period, resulting in greatly diminished plaque formation. Additionally, continual culture with PP compounds resulted in greater inhibition (Figure 4B), consistent with its ability to block the multiple rounds of invasion and egress that occur during plaque formation, although it is likely that tachyzoites predominate during these longer-term assays.

Mouse Pharmacokinetic Studies. We examined the pharmacokinetics (PK) of several PP inhibitors in mice following either iv injection or po administration in mice. Compounds 1 and 2 showed reasonable oral bioavailability (F) ranging from ~25% to 30%, C_{max} levels, and moderate clearance (CL) values that were below the level of single pass circulation through the liver in mouse (~90 mL/(min·kg)) (Table 2). Compound 10 showed a higher clearance rate but had similar half-life (T_{1/2}) to 1 and 2 of ~1.5–2 h (Table 2). However, this compound suffered from poor oral bioavailability (Table 2). Although compound 13 had greater in vitro stability in microsomes (Table 1), it also displayed rapid clearance in vivo, perhaps due to efflux as

indicated above. Compound 13 also showed lower C_{max} values and high tissue exposure as evidenced by its volume of distribution (V_{ss}) (Table 2). Finally, compound 24 showed the best combination of properties with good C_{max} following oral dosing, moderate clearance rate, T_{1/2} ≈ 1.5 h, and very high oral availability (e.g., ~94%) (Table 2). These collective properties of compound 24 provided the best PK profile and highest values for AUC, reflecting prolonged serum exposure following oral dosing.

Based on these favorable properties, we examined the PK of 24 in mice using increasing oral doses from 10, 25, and 50 mg/kg (Figure 4C). At higher dose, 24 showed a two-phase decay curve in plasma, with rapid initial drop followed by a more gradual plateau that was seen at 25 and 50 mg/kg (Figure 4C). Based on its protein binding properties (12% free in serum), the concentration of compound 24 in serum would need to be 2.08 μ M, for the free value to attain a level equivalent to the in vitro EC₅₀ of ~0.250 μ M. This corresponds to a value of 856 ng/mL in serum, as shown by the red line in Figure 4C. The protein bound fraction in brain was slightly higher at 97.2% or 2.8% free, and the ratio of total compound in the CNS vs serum was 5.6, for an effective brain vs plasma ratio ~1.3. Consequently, we would expect that the free concentration of compound 24 in the brain was approximately the same or slightly higher than that shown for serum in Figure 4C.

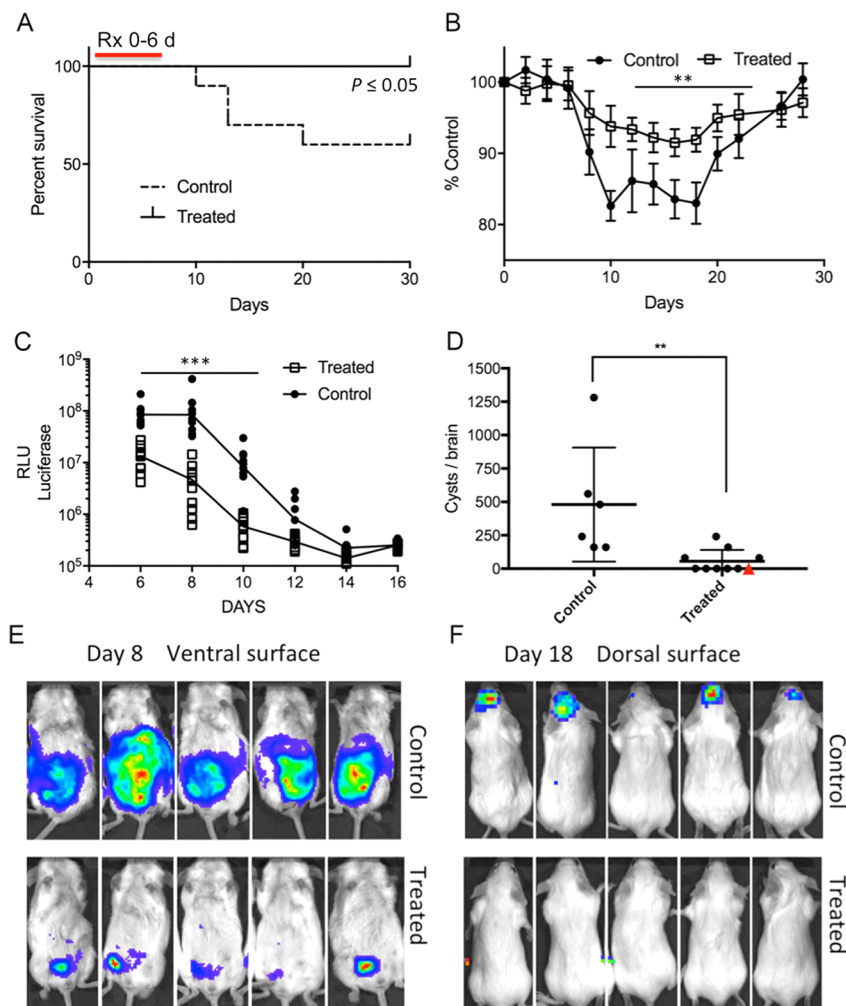


Figure 6. In vivo treatment of acute toxoplasmosis with compound 24. (A) Survival curve of mice infected with ME49-FLUC strain parasites and treated with compound 24 (treated) vs vehicle control (control) as monitored for 30 days. Animals were infected with 5000 tachyzoites by ip injection on day 0. At 24 h postinfection, animals were given compound 24 at 50 mg/kg or vehicle control, followed by a second dose of 25 mg/kg 12 h later, and then treated with 25 mg/kg BID for 5 additional days. Mantel–Cox test, $P \leq 0.05$. (B) Weight loss of infected animals shown in panel B. Values are reported as % Control, which refers to the average weight at day 0 for each group treated separately. (C) Bioluminescence imaging of parasite numbers in animals shown in panel A. Whole body imaging was used to determine the mean intensity of luciferase signal, which is expressed as relative light units (RLU). Individual animals shown by symbols; median values graphed in the lines. Student's *t* test with Holm–Sidak correction for multiple tests, *** $P \leq 0.001$. (D) The number of cysts in surviving animals from panel A were determined by counting aliquots of brain homogenate. Means \pm SD, $n = 6\text{--}9$. Threshold for detection = 40 cysts. Red triangle denotes animal where bioassay was negative indicating it was cured. Mann–Whitney nonparametric test, ** $P \leq 0.01$. (E) Bioluminescence imaging of representative control and treated mice from panel A imaged at day 8. (F) Bioluminescence imaging of control and treated mice from panel A imaged at day 18.

Treatment of Acute Toxoplasmosis. Based on its favorable PK parameters, we tested compound 24 for its ability to prevent toxoplasmosis in the mouse model. Following an initial loading dose of 50 mg/kg, 24 was administered orally at 25 mg/kg BID for 6 days, beginning 24 h after challenge with tachyzoites of the ME49 strain of *T. gondii*. Treatment with 24 decreased the frequency of lethal infection (Figure 6A), and this was associated with reduced weight loss (Figure 6B) and with decreased tissue burdens of the parasite, as revealed by bioluminescent imaging (Figure 6C). Consistent with a decrease in acute burden, there were fewer tissue cysts formed in the brains of chronically infected mice following treatment with 24 (Figure 6D). The dramatic ability of 24 to decrease dissemination was further shown by bioluminescent imaging, where control animals showed extensive expansion of the parasite with in the peritoneum at day 8 and spread to the head at day 18 (Figure 6E,F). In contrast, treated mice were able to restrict the

growth of the parasite to the site of injection and did not show detectable signal in the head (Figure 6E,F). Following treatment with 24, many animals showed tissue cyst levels below the levels of detection (40 cysts per brain) (Figure 6D). These animals were subsequently bioassayed by oral feeding of 20% of their brain homogenate into a naive interferon gamma receptor knock out mouse (*Ifngr1*^{-/-}). Although 5 of 6 recipient animals succumbed to infection, reflecting a low level of chronic infection in the donor, one remained alive, indicating that compound 24 treatment had resulted in a complete cure in this animal (Figure 6D, red triangle).

Treatment of Reactivated CNS Toxoplasmosis. To determine whether compound 24 could prevent reactivation of chronic toxoplasmosis, we utilized mice lacking the IFN γ receptor (i.e., *Ifngr1*^{-/-}), which are highly susceptible and rapidly succumb to infection.³⁷ Treatment of such animals with sulfadiazine will suppress the growth of tachyzoites, while

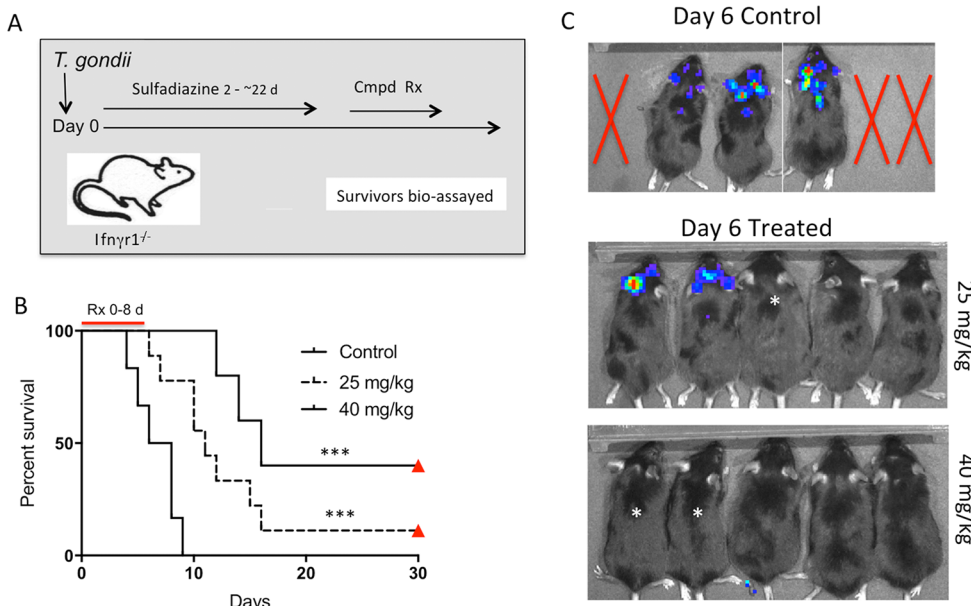


Figure 7. In vivo treatment of reactivation of CNS toxoplasmosis. (A) Schematic for treatment during reactivation in an immunocompromised mouse. Ifngr1^{-/-} mice were infected with 10 cysts of the ME49-FLUC strain and treated from day 2–22 with sulfadiazine in the drinking water. Two days (48 h) after removal of sulfadiazine, animals were treated po with compound 24 or vehicle control (control, $n = 6$) for 8 days. Animals in one group ($n = 9$) received a loading dose of 50 mg/kg followed by 25 mg/kg 12 h later and then 25 mg/kg BID for seven additional days. A second group of animals ($n = 5$) received 40 mg/kg BID for 8 days. (B) Animals were evaluated for survival and imaged for bioluminescence over a period of 30 days. Treated mice survived significantly longer than controls, log-rank, Mantel–Cox test, $P < 0.001$ (***) . Animals that survived in the treated groups (red triangles) were negative by bioassay, indicating they were cured. (C) Bioluminescence imaging at day 6 indicates that a number of control animals that have perished (red X) and remaining animals show a positive signal in the head and upper thorax. In contrast, all treated mice were alive and mice treated with 25 mg/kg show reduced signals while those treated with 40 mg/kg showed no sign of activation. Animals marked * were determined to be cured based on bioassay at the end of the experiment.

allowing the development of chronic tissue cysts.³⁸ Subsequent removal of sulfadiazine results in rapid reactivation, characterized by CNS encephalitis, pneumonia, and death.³⁸ We injected Ifngr1^{-/-} mice with a type II strain capable of causing chronic infection and treated them from day 2 to 22 with sulfadiazine in the drinking water, which prevented otherwise lethal infection. Following removal of sulfadiazine (48 h later), mice were treated with compound 24 at a dose of 25 or 40 mg/kg BID or with vehicle only control by oral gavage for 8 days (Figure 7A). Withdrawal of sulfadiazine from the control animals lead to rapid reactivation of chronic infection and led to death of the control mice within 10 days (Figure 7B). In contrast, treatment with compound 24 prolonged survival (Figure 7B). We also monitored the progression of infection using bioluminescence. At the beginning of the treatment period, all of the animals were negative for bioluminescence, consistent with the infection being chronic. Monitoring of the control animals revealed that reactivation was first centered in the CNS, with later spread to the lungs prior to death (Figure 7C). In contrast to the rapid expansion of parasites seen in control mice, the bioluminescence signal was muted in compound 24 treated mice, and reactivation was significantly delayed (Figure 7C). Consistent with this delay in reactivation, compound 24 treated mice survived significantly longer (Figure 7B). One animal treated with compound 24 at 25 mg/kg and two animals treated at 40 mg/kg remained negative for bioluminescence signals and survived for an additional 22 days after removal of compound (red triangles in Figure 7B). Subsequent bioassay of brain homogenates from these treated mice into naive Ifngr1^{-/-} mice did not result in transfer of infection, confirming that these animals had been cured (Figure 7B).

■ DISCUSSION

In previous work, we demonstrated that PP inhibitors containing *meta* chloro benzyl substituents at C3 of the PP core provide potent inhibition of CDPK1 in *T. gondii*.³⁶ However, when coupled with isopropyl or *t*-butyl at R₂, these compounds suffer from metabolic instability.³⁶ Our profiling of host kinases here also reveals that compounds like 1 lack specificity, and this is also likely true of other related derivatives that share this basic architecture. To alleviate this problem, we altered the linkage connecting R₁ to C3 from a methylene to a heteroatom consisting of O, S, or N. An ether linkage proved most optimal in increasing stability and selectivity, while compounds with a thioether linkage were typically less active and compounds with an amine linkage were less selective. The reasons for these differences are not exactly clear as cocrystal structures of these analogs showed very close overlap of the analogs in the binding pocket. The lower activity of the thioether linkage may relate to the bulkier nature of this atom within the linker, which is very close to the hinge region in the crystal structure. We have previously shown that even subtle modification to this linker, such as substitution of fluorine for hydrogen, ablates activity.²³

By combining the ether linkage at C3 with a methylpiperidine at R₂, we achieved further gains in specificity, with only modest loss of potency. Other modifications to R₂, such as including a pyridine or methylation of the piperidine nitrogen, ablated activity suggesting that the unsubstituted alkyl amine is critical for the potency. Indeed a cocrystal structure of compound 13 revealed that this amine is important for forming a hydrogen bond with glutamate 135 in the ribose-binding region, likely stabilizing the interaction of the compound with the ATP-binding pocket. Addition of the piperidine group in the

scaffold described here also resulted in dramatic improvement in specificity over host kinases compared to the initial lead compounds **1** and **2**. Compounds **13** and **24** only potently inhibited a single human kinase, CK1 ϵ , under conditions tested here. Surprisingly, CK1 ϵ is also sensitive to other PP analogs including 1-NM-PP1 and 1-NA-PP1, despite its methionine gatekeeper, which is normally a hallmark for resistance to such analogs.³⁹ The sensitivity of CK ϵ to PP analogs has been attributed to an unusual flexibility in the M side-chain that allows access of bulky PP analogs into the ATP-binding pocket.⁴⁰ Further modification of the PP scaffold may result in inhibitors that would retain potency for CDPK1 over CK ϵ . However, this off target activity may be less of an issue in vivo since compound **24** retains good potency against parasite growth in a cell-based assay, while off target activity against CK ϵ drops appreciably at higher ATP levels.

Despite the improvements in specificity achieved with the piperidine analogs, these charged primary amines suffered from efflux problems in our study, likely due to the high pK_a .³⁴ Addition of di-F in the piperidine ring decreased the predicted pK_a and eliminated the efflux problem, consistent with previous examples in other scaffolds.³⁴ Previous experimental measurements of piperidine amines with fluoro substituents,³⁴ combined with computational predictions of the compound **24** piperidine amine pK_a suggest that the piperidine amine in compound **24** is partially protonated at physiological pH. Based on these properties and its potency, we would predict that compound **24** is still able to form a H-bond with E135 in CDPK1. Unfortunately, modification of di-F *meta* to the amine in the piperidine was also associated with some loss of metabolic stability, which likely limited its in vivo efficacy. We did not explore modification with fluorine-directed modifications at other positions in the piperidine ring, but conceivably some of these may have a more optimal combination of features.

One of the goals of our study was to obtain molecules with better metabolic stability to improve in vivo PK properties for treating acute and chronic toxoplasmosis in the mouse. Compound **24** exhibited many of the desired properties in terms of PK in the mouse. Although C_{max} levels were high, it was relatively rapidly cleared from serum, likely as a consequence of metabolism in the liver as the half-life in microsomes was relatively short. This was partially offset by high oral availability and moderate protein binding, resulting in reasonable serum profiles and good AUC profiles. However, we were only able to obtain free serum levels that exceeded the EC₅₀ based on free drug for a period of ~2 h after oral dosing in the mouse. Nonetheless, dosing schemes of 25–50 mg/kg were able to decrease acute infection, preventing weight loss and death in a majority of immunocompetent animals. Additionally, treatment during acute infection resulted in dramatically lower cyst counts during chronic infection, likely as a consequence of decreasing dissemination to the CNS. Indeed, treatment was sufficient to provide a complete cure in one animal with no evidence of chronic infection.

Although previous studies have largely focused on the acute infection model, the primary concern for immunocompromised patients is the reactivation of prior chronic infections.⁹ Here we modeled this situation using severely immunocompromised Ifngr^{-/-} mice, which are highly susceptible to *T. gondii* infection.³⁷ As Ifngr^{-/-} mice completely lack the ability to respond to IFN γ , a critical mediator of host defense, it is likely that a single tissue cyst or single viable organism is capable of causing lethal infection in this model. Hence they provide an extremely

sensitive measure of the ability of compounds to cure infection. Treatment with atovaquone³⁸ or artemisinin⁴¹ derivatives is able to prolong survival of such severely immunocompromised mice, but treated animals ultimately always succumb to infection following removal of these drugs. Similarly, treatment with sulfadiazine is only able to prevent lethal infection in this model, but not eliminate the tissue cysts, such that when it is removed, animals quickly succumb due to reactivation of rapidly growing tachyzoites. Treatment with compound **24** prolonged survival of Ifngr^{-/-} mice and resulted in a radical cure in some animals, a result not previously seen with other compounds. The efficacy of compound **24** in this model likely stems from its ability to block tachyzoite invasion and egress, but it was also able to block bradyzoite invasion in vitro, suggesting it may directly affect the formation and turnover of cysts in vivo. Other PP analogs have been reported to reduce the chronic cyst burden in infected mice, albeit at very high serum doses, which exceed the level where they are selective for CDPK1.¹⁹ In contrast, compound **24** retains antitoxoplasma activity at very modest serum levels, which are well within the range where it is selective for CDPK1 in *T. gondii*.^{12,23}

CONCLUSIONS

CDPK1 is an essential kinase in *T. gondii* and hence has been the focus of development of potent and selective inhibitors. Here we report new PP inhibitors that were designed to improve metabolic stability and specificity for CDPK1. The optimal molecule in this series, compound **24**, showed low nanomolar inhibition of CDPK1 in vitro, submicromolar inhibition of parasite growth in vitro, and improved metabolic stability. In vivo administration of this analog, which showed excellent oral availability and moderate PK parameters, decreased the severity of acute infection, reduced tissue cyst levels, and delayed reactivation of chronic toxoplasmosis in the mouse. Additionally, compound **24** is remarkable in being able to completely cure a portion of immunocompromised animals. As radical cure is currently not possible for humans infected with *T. gondii*, compounds that can achieve this goal with higher efficacy would greatly enhance the potential utility of PP analogs for treatment of toxoplasmosis. Collectively, these advances underscore the utility of the PP scaffold as a new therapeutic agent for treatment of acute and chronic toxoplasmosis.

EXPERIMENTAL SECTION

Chemical Synthesis. Starting materials, solvents, and reagents obtained commercially were reagent grade and were used without further purification. NMR spectra were obtained at the University of California, San Francisco, NMR facility: ¹H NMR were recorded on a Bruker AvanceIII HD 400 at 400 MHz, and ¹³C spectra were recorded on a Bruker AvanceIII HD 400 at 400 MHz or a Bruker Advance DRX500. High-resolution mass spectra (HRMS) were acquired by electrospray ionization (ESI) in positive ion mode using Finnigan LTQ FT mass spectrometer (Thermo) at the QB3/Chemistry Mass Spectrometry Facility (University of California, Berkeley). Samples were directly injected into ESI source via syringe pump with flow rate 5 μ L/min. Reactions were monitored by thin layer chromatography (TLC), using Merck silica gel 60 F254 glass plates (0.25 mm thick). Flash chromatography was conducted with Teledyne Isco RediSep Rf silica flash cartridges on a Teledyne Isco CombiFlash Rf+. All RP-HPLC were performed with a Waters 2545 binary gradient module equipped with an XBridge prep C18 column using H₂O + 0.1% formic acid and CH₃CN + 0.1% formic acid (5–95% gradient) while monitoring at 254 nm. All final compounds were >95% pure as measured by liquid chromatography–mass spectrometry (LCMS) using a Waters Acuity UPLC/ESI-TQD BEH C18 (1.7 μ m) column using H₂O + 0.1% formic acid and CH₃CN + 0.1% formic acid (5–95% gradient) over 1.8 min at

600 μ L/min. Full compound characterization details are presented in the Supporting Information. All compounds reported here were screened for Pan Assay Interference (PAINS) and found to pass all the filters contained in the FAF-Drugs4 Web server (<http://fafdrugs4.mti.univ-paris-diderot.fr/>).

Parasite Strains and Cell Lines. Tachyzoites of *T. gondii* strains were grown in monolayers of human foreskin fibroblasts (HFF) maintained in complete medium (DMEM containing 10% FBS, 10 mM glutamine, and 10 μ g/mL gentamycin) at 37 °C in 5% CO₂. Following natural egress, tachyzoites were purified in HBSS containing 10 mM HEPES, 0.1 mM EGTA, and separated from host debris using 3.0 micro polycarbonate membrane filters, followed by centrifugation at 400g. HFF monolayers obtained from an anonymous donor were provided by Dr. John Boothroyd's laboratory (Stanford University). All strains and host cell lines were determined to be mycoplasma negative using the e-Myco plus kit (Intron Biotechnology).

Enzyme Expression and Purification. Full-length *T. gondii* CDPK1 enzyme was expressed with a C-terminal His tag in pET22b(+), as described previously.¹² CDPK1 was expressed in BL21 (DE3)-V2RpAcYc-LIC+LamP *E. coli*, which contains the LamP phosphatase. A cDNA fragment encoding human Src (hSrc) kinase domain amino acids 254–536 was amplified using the primers Scr-F (GATATA-CATATGCAGACTCAGGGCCTGGC) and Scr-R (GTGGTG-CTCGAGGAGGTTCTCCCC) and cloned into pET22b using restriction enzymes *Nde*I and *Xho*I. hSrc containing a Thr gatekeeper residue (equivalent of Thr338 in the full length sequence of the c-Src allele) was expressed in BL21 (DE3)V2RpAcYc-LIC+LamP *E. coli*, which contains the LamP phosphatase. Following overnight growth in Terrific Broth at 37 °C, the culture was diluted 1:100 and grown for 3 h at 37 °C (OD 0.6–0.8), then induced with 0.3 mM IPTG during overnight growth at 15 or 30 °C. Cells were lysed by sonication, and soluble proteins were purified using HIS-select Nickel Affinity Gel. Purified proteins were dialyzed (50 mM Tris-HCl, pH 7.5, 150 mM NaCl), and stored in 25% glycerol containing 0.5 mM DTT at –80 °C. Protein purity and concentrations were determined by SDS-PAGE and staining with SYPRO Ruby (Invitrogen).

Crystallography Method. For the purpose of crystallization, recombinant *TgCDPK1* was expressed, purified, and set up in crystal trial with inhibitors as previously described.¹⁴ Diffracting crystals were obtained by cocrystallization with compounds 3 (PDB code: SW9E), 1 (PDB code: SW8R), 2 (PDB code: 41H8), 13 (PDB code: SW80), and 4 (PDB code: SW91). Crystallographic data were collected at beamline 19ID of Argonne National Laboratory's Advanced Photon Source (<http://www.sbc.anl.gov/index.html>) and processed using HKL-3000.⁴² All structures were solved using Phaser for molecular replacement and the previously deposited *TgCDPK1* coordinates (PDB code: 41H8) as a search model. The models were refined using Buster⁴³ and REFMAC⁴⁴ combined with iterative manual model building using the molecular graphics program Coot.⁴⁵ The geometry of all final models was checked using MolProbity.⁴⁶ Crystallographic details and refinement statistics are summarized in Table S1. Atomic coordinates and experimental data will be released on publication.

Homology Modeling. Compound 24 was modeled using the cocrystal structure of compound 13 (PDB code: SW9E) in Molecular Operating Environment (MOE) version 2015.1 by Chemical Computing Group.⁴⁷ Difluorine was added to the piperidine of compound 13 using the ligand builder to create compound 24, and the structure was prepared and minimized using LigX with the Amber10-EHT force field (used Protonate3D for protonation, allowed ASN/GLN/HIS “Flips” in Protonate3D, deleted water molecules farther than 4.5 Å from compound 24 or CDPK1; tethering parameters: receptor strength at 5000 to minimize large changes to the CDPK1 backbone, fixed atoms farther than 8 Å away from compound 24, hydrogens close to compound 24 not fixed, and refined compound 24–CDPK complex to an RMS gradient of 0.1 kcal/(mol·Å)).

Enzyme Assays and IC₅₀ Values. CDPK1 activity was monitored based on phosphorylation of syntide-2 peptide (Calbiochem), which was detected using mAb MS-6E6 (MBL Intl, Corp) using an ELISA protocol described previously.²³ Kinase reactions were conducted at 30 °C for 20 min in 20 mM HEPES, pH 7.5, 10 mM MgCl₂, 1 mM DTT,

2.5 mM CaCl₂, 0.1 mM EGTA, 0.005% Tween 20. Reactions were conducted using 25 μ M ATP (the K_m for the enzyme) using 140 ng of kinase per reaction. To determine the potency of inhibitors, duplicate wells were treated with a range of compound concentrations from 10 μ M to 0.5 nM. Inhibitors were preincubated with the enzyme in the reaction buffer for 10 min before addition of ATP. Individual IC₅₀ values were determined from two or more independent biological replicates and are reported as mean values. Src activity was monitored by phosphorylation of the Abltide peptide (EAIIYAAPFAKKK, Enzo Life Sciences), which was detected using a monoclonal antibody to phosphotyrosine (Sigma) using an ELISA protocol similar to that used for CDPK1 above. Kinase reactions were conducted in 50 mM Tris-HCl, pH 7.5, 10 mM MgCl₂, 2.5 nM MnCl₂, 0.2 mM DTT, 0.5 mM EGTA. Reactions were conducted using 5 μ M ATP (the K_m for the enzyme) using 75 ng of kinase per reaction. Compounds were tested at 10 μ M in duplicate, in two biological replicates, and values are reported as mean \pm SD. For compounds that showed >50% inhibition at 10 μ M, serial dilutions from 10 μ M to 0.5 nM were tested in duplicate to derive IC₅₀ values.

CK1 ϵ (ThermoFisher) activity was monitored based on phosphorylation of dephosphorylated casein (Sigma-Aldrich) under the following conditions: 50 mM TRIS (pH 7.4), 10 mM MgCl₂, 0.4 mg/mL casein, 2.5 mM DTT, 2% DMSO, 0.1 mg/mL BSA, 2 μ M ATP (K_{m,app}), 1 μ Ci ³²P-ATP (PerkinElmer), 5 nM CK1 ϵ . Additional activity assays were done at 100 μ M ATP with 10 nM kinase. To determine the potency of inhibitors, duplicate wells were treated with a 10-fold dilution of compound from 200 μ M to 200 pM. Inhibitors were preincubated with the enzyme in the reaction buffer for 15 min before addition of ATP and ³²P-ATP. Upon completion of the reaction (10 min for K_{m,app}, 55 min for 100 μ M ATP), 3 μ L was spotted onto P81 paper. The paper was dried for 5 min under a heat lamp followed by 1 \times 30 s wash and 6 \times 5 min washes in 1% phosphoric acid. The paper was dried for 15 min under a heat lamp followed by overnight exposure to a phosphor screen imaged on a Typhoon 9500. Intensities were quantified using densitometry, and IC₅₀ values were determined from quantification of two independent biological replicates of triplicate dose response determined by fitting the data to a sigmoid function in Prism 7.0 (GraphPad Software) and are reported as mean values.

Kinome Screen. Human kinome profiling was conducted using the ThermoFisher Scientific SelectScreen ACCESS program to profile 489 kinases utilizing three assay formats: Z'-LYTE (284 kinases), Adapta (39 kinases), and LanthaScreen (166 kinases). Z'-LYTE and Adapta yield % inhibition values based on the mean of 2 points that measure the ability of the compound to inhibit an active kinase. LanthaScreen yields % displacement values based on the mean of 2 points that measure the ability of the inhibitor to displace a tracer bound to an inactive or weakly active kinase. Inhibitors were screened at 1 μ M.

Parasite Growth Assays and EC₅₀ Values. Parasite growth inhibition assays were conducted using the type I RH strain, 2F clone, which expresses bacterial β -galactosidase (β -gal), as described previously.²³ Compounds dissolved in DMSO at 10 mM stocks were diluted in medium to two times final concentrations and added to an equal volume of medium containing 5×10^2 parasites and incubated for 20 min. Mixtures of compounds (ranging from 10 μ M to 0.01 nM) containing 0.1% (v/v) DMSO or DMSO alone was added to monolayers of HFF cells grown in 96 well plates, centrifuged at 300g for 5 min, and returned to culture at 37 °C, 5% CO₂. After 4 h, the plates were washed to remove extracellular parasites and compounds and then returned to culture for 72 h. At the end of the incubation period, the monolayer was lysed in 1% Triton X-100 and β -gal activity monitored using 1 mM chlorophenol red- β -D-galactopyranoside by absorption at 570 nm, as described previously.²³ Individual EC₅₀ values were determined from three or more independent biological replicates and are reported as mean values.

Host Toxicity Assays. HFF cells were plated in complete medium and allowed to adhere for 4 h at 37 °C, 5% CO₂. Compounds diluted to 10 μ M in 0.1% (v/v) DMSO or DMSO alone was then added, and cells were incubated for an additional 72 h. Following the incubation period, samples were evaluated using a cell proliferation assay (CellTiter 96 Aqueous Non-Radioactive Cell Proliferation Assay, Promega Corporation).

As a positive control, mitomycin C (10 μ M) was included in each plate. Compounds were tested in duplicate, in two biological replicates, and values are reported as means \pm SD.

In Vitro Analysis of Uptake, Efflux, Metabolism, and Protein Binding. Assays to monitor uptake and efflux of compounds by polarized epithelial cells were conducted by Absorption Systems Inc. (Exton, PA, USA). In brief, Caco-2 cells (Clone C2BBel from ATCC) were grown to confluence on collagen-coated polycarbonate membranes on transwell plates. Permeability assays were conducted in Hank's balanced salt solution, containing 10 mM HEPES, 10 mM glucose, pH 7.4. Compounds were added at 5 μ M to the apical (A) vs basolateral (B) side, and duplicate samples were taken at 120 min. Samples were analyzed by LC-MS/MS and expressed as apparent permeability (P_{app}) for uptake (A to B) vs efflux (B to A) and efflux ratio ($P_{app}(B \text{ to } A)/P_{app}(A \text{ to } B)$).

The stability of compounds in the presence of rat or mouse liver microsomes was conducted by Absorption Systems, Inc. In brief, rat liver microsomes or mouse rat liver microsome were incubated with compounds at 1 μ M in a shaking water bath for 60 min. Aliquots were withdrawn at intervals, extracted, and analyzed by LC-MS/MS to evaluate the remaining parent compound. Half-lives were calculated using a single-phase exponential decay equation (Graph Pad). Intrinsic clearance was calculated as $CL_{int} = k/P$, where k is the elimination rate constant and P is the protein concentration in the assay. For plasma protein binding, compounds were incubated at 5 μ M in CD-1 mouse plasma, and protein bound fractions were monitored by equilibrium dialysis.

In Vivo Pharmacokinetic Studies. Pharmacokinetic (PK) studies were conducted by Sai Life Sciences Limited (India). Compounds were administered orally in 50% PEG-400 in PBS, while for iv administration, compounds were dissolved in 20% PEG-400–PBS. Mean plasma concentrations were determined following a single iv dose of 3 mg/kg in male Swiss Albino mice by sampling at 0.05, 0.25, 1, 2, 4, and 8 h. Separately, male mice were used for monitoring mean plasma concentrations following single oral dose of 10 mg/kg with similar time points. Separate animals were used to determine the brain distribution relative to plasma levels at 1 h following a single oral dose of 10 mg/kg. Selected compounds were tested for dose response of plasma concentrations following single or multiple oral administration of a single dose of 10, 25, and 50 mg/kg at time intervals of 0.25, 1, 2, 4, 8, and 24 h. Plasma samples were separated, processed by precipitation in acetonitrile, and analyzed by LC-MS/MS. Pharmacokinetic parameters, including those for plasma versus brain, and oral bioavailability were calculated with the noncompartmental analysis tools of the Phoenix WinNonLin (v6.3).

Animal Studies. Animals were obtained from Jackson Laboratories and housed at Washington University in accordance with the U.S.A. Public Health Service Policy on Humane Care and Use of Laboratory Animals. Animals were maintained in an Association for Assessment and Accreditation of Laboratory Animal Care approved facilities, and protocols were approved by the Institutional Animal Studies Committee at the School of Medicine, Washington University in St. Louis.

Ex Vivo Bradyzoite Treatment Assays. Adult (8–12 weeks old) female CD1 mice were infected with tachyzoites of the Pru Δ hxg Δ ku80, LDH2-GFP (PRU-GFP),⁴⁸ or ME49 Δ hx::FLUC⁴⁹ strains expressing firefly luciferase (FLUC)⁴⁹ and allowed to develop chronic infections. Adult (8–12 weeks old) CBA/J mice were orally infected with 10–20 tissue cysts of the ME49 Δ hx::FLUC strain. At 3–6 weeks post-inoculum, brains were isolated from 2 to 3 animals, and tissue cysts were purified from brain homogenate by Percoll gradient, as previously described.¹¹ A serological pipet was used to isolate the ~9.0 mL of gradient between the erythrocyte layer and the brain homogenate layer after the initial centrifugation step (1200g for 15 min at 4 °C). Following purification, cysts were resuspended in acid-pepsin solution (170 mM NaCl, 60 mM HCl, 0.1 mg/mL pepsin (1:10000 activity)), incubated for 10 min at 37 °C, and then neutralized by addition of sodium carbonate solution (94 mM). Liberated bradyzoites were inoculated into parallel 6-well plates containing HFF monolayers with compounds (constant treatment vs washout). At 4 h postinfection, the washout 6-well plate was rinsed 3 times in fresh media to remove cell debris and noninvaded parasite and returned to incubator with fresh culture medium lacking compound. The constant treatment plate was allowed to incubate

without washing. Plates were incubated for 10–14 days prior to ethanol fixation and staining with 0.1% crystal violet stain, and plaques were counted using an Axio Observer.D1 microscope under 2.5 \times magnification.

Treatment during Acute Challenge Studies. Adult (8–12 weeks old) female Balb/C mice were infected with 5000 tachyzoites of the type II ME49 Δ hx::FLUC line by ip injection. At 24 h postinfection, animals were dosed with compounds formulated in 25% PEG–PBS containing 5% DMSO or 25% PEG-400–PBS–5% DMSO alone, by oral gavage, and treatment was continued for 6 days. Treated mice received on day 1 an initial loading dose of compound 24 at 50 mg/kg in the morning, followed 12 h later by a second dose of 25 mg/kg, and then 25 mg/kg BID for 5 additional days. Bioluminescence imaging (see below) was used to monitor infection from day 6 to 20, and weight loss and survival were tracked over the first 30 days. At the end of 30 days, tissue cysts in the brain were quantified by staining with *Dolichos biflorus* lectin that was labeled with FITC, and microscopic examination, as described previously.⁵⁰ For samples where no cysts were observed (lower threshold = 40 per brain), residual infection was tested by bioassay into a naive recipient. For bioassay experiments, 200 μ L of brain homogenate was injected ip into a recipient Ifngr1 $^{-/-}$ mouse, which lacks the ability to control parasite proliferation and readily succumbs to infection.³⁷

Treatment during Reactivation of Chronic Toxoplasmosis. To provide a model for treatment during reactivation of chronic infection, we used a modification of a previously published protocol.^{38,41} Male and female Ifngr1 $^{-/-}$ mice were orally infected with 5 cysts of the type II ME49 Δ hx::FLUC line, obtained from the brains of chronically infected wild type CD-1 mice. Animals were treated with sulfadiazine (0.25 g/L in the drinking water) from day 2 to 22. Two days (48 h) after removal of the sulfadiazine, compound 24 formulated in 25% PEG-400–PBS containing 5% DMSO or 25% PEG-400–PBS–5% DMSO alone (control) was administered by oral gavage for a total of 8 days. One group of treated mice received on day 1 an initial loading dose of compound 24 at 50 mg/kg in the morning, followed 12 h later by a second dose of 25 mg/kg, and then 25 mg/kg BID for 7 additional days. A second group of animals received compound 24 at 40 mg/kg BID for 8 days. Animals were monitored for weight loss, bioluminescence imaging, and survival for 30 days. At the end of 30 days, animals were examined for presence of cysts in the brain and by bioassay by inoculation of brain homogenate (200 μ L of 1 mL) into a naive recipient Ifngr1 $^{-/-}$ mouse, as described above. There were no differences in outcome associated with the sex of animals.

Bioluminescence Imaging. Animals were monitored for bioluminescence using a Xenogen IVIS200 instrument, and images were analyzed using the Xenogen Living Image software (Caliper Life Sciences). Mice were anesthetized using 2% isoflurane and injected ip with d-luciferin (Biosynth AG) at 150 mg/mg just prior to imaging.

Statistical Analyses. Mathematical and statistical analyses were conducted in Prism (GraphPad). IC₅₀ and EC₅₀ values were determined using normalized, log-transformed (concn) data fit with nonlinear regression analysis based on sigmoidal dose–response curves with variable slope. For correlating IC₅₀ to EC₅₀ values, r^2 values were generated using linear regression analysis. Mean values for inhibition of bradyzoite plaque formation were analyzed using two-way ANOVA with Dunnett's correction for multiple comparisons. Survival curves were plotted as Kaplan–Meier survival curves, and significance determined by the Mantel–Cox test. Mean values for bioluminescence and weight loss were compared using Student's *t* test with Holm–Sidak correction for multiple tests. The average numbers of cysts per brain were compared using a Mann–Whitney nonparametric test for non-normally distributed data with unequal variance. For all tests, a minimum value of $P \leq 0.05$ was considered significant, and individual values are given in the figure legends.

■ ASSOCIATED CONTENT

S Supporting Information

The Supporting Information is available free of charge on the ACS Publications website at DOI: [10.1021/acs.jmedchem.7b01192](https://doi.org/10.1021/acs.jmedchem.7b01192).

Compound synthesis, characterization, metabolism analysis, X-ray crystallography information, kinome profiling ([PDF](#))

Compound 24 homology model ([PDB](#))
Molecular formula strings ([CSV](#))

Accession Codes

The structure factors and pdb coordinates have been deposited at the protein databank (PDB) with the coordinates 4IHP, 5W8R, 5W80, 5W9E, and 5W91. Compound 24 was modeled using the co-crystal structure of compound 13 (PDB code: 5W9E). Authors will release the atomic coordinates and experimental data upon article publication.

AUTHOR INFORMATION

Corresponding Author

*E-mail: sibley@wustl.edu. Phone: 314-362-8873.

ORCID

Kevan M. Shokat: [0000-0002-6900-8380](https://orcid.org/0000-0002-6900-8380)

L. David Sibley: [0000-0001-7110-0285](https://orcid.org/0000-0001-7110-0285)

Present Address

[#]Achaogen Inc., One Tower Place, #300, South San Francisco, CA 94080.

Author Contributions

▀ J.B., M.S.D., and Q.W., listed alphabetically, contributed equally. F.U.R. and M.S.L. performed the chemical syntheses and physical characterization of the compounds described here. J.B. performed the in vitro cell-based assays for parasite and host cell growth inhibition. M.S.D. and S.L. performed the enzyme purification and enzyme assays. Q.W. conducted the animal studies with assistance from L.D.S. N.J. and J.B.R. performed the ex vivo tissue cyst experiments. A.R.M. purified select chemicals for in vivo studies. J.W.J. provided advice on chemical synthesis. M.E.B. and R.H. performed the structural studies. L.D.S. and K.M.S. supervised the research. F.U.R. and L.D.S. performed data analyses, generated the figures, and wrote the manuscript with input from all authors.

Notes

The authors declare no competing financial interest.

ACKNOWLEDGMENTS

We are grateful to Keliang Tang who performed the initial studies on enzyme kinetics and established the enzyme assays and to Martin John Rodgers for his early support of this project. We also thank John R. Walker of the Structural Genomics Consortium for verifying the crystallographic structures and for their deposition into the Protein Data Bank and the UCSF NMR Lab and QB3/Chemistry Mass Spectrometry Facility (University of California, Berkeley) for access to instrumentation for compound characterization. Supported by a grant from the NIH (AI094098 to K.M.S. and L.D.S.). The compounds reported here are the subject of patent applications filed by UCSF and Washington University.

ABBREVIATIONS USED:

ANOVA, analysis of variance; β -gal, β -galactosidase; BID, bis in die (twice a day); CDPK1, calcium dependent protein kinase 1; CNS, central nervous system; EC₅₀, 50% effective concentration; ELISA, enzyme-linked immunosorbent assay; HAART, highly active antiretroviral therapy; HFF, human foreskin fibroblast; HIV, human immunodeficiency virus; IC₅₀, 50% inhibitor concentration; FLUC, firefly luciferase; SAR, structure–activity relationship

REFERENCES

- (1) Montoya, J. G.; Liesenfeld, O. Toxoplasmosis. *Lancet* **2004**, *363*, 1965–1976.
- (2) Dennis, A. M.; Napravnik, S.; Sena, A. C.; Eron, J. J. Late entry to HIV care among Latinos compared with non-Latinos in a southeastern US cohort. *Clin. Infect. Dis.* **2011**, *53*, 480–487.
- (3) Kiderlen, T. R.; Liesenfeld, O.; Schurmann, D.; Schneider, T. Toxoplasmic encephalitis in AIDS-patients before and after the introduction of highly active antiretroviral therapy (HAART). *Eur. J. Clin. Microbiol. Infect. Dis.* **2011**, *30*, 1521–1525.
- (4) Oliveira, J. F.; Greco, D. B.; Oliveira, G. C.; Christo, P. P.; Guimaraes, M. D.; Oliveira, R. C. Neurological disease in HIV-infected patients in the era of highly active antiretroviral treatment: a Brazilian experience. *Rev. Soc. Bras. Med. Trop.* **2006**, *39*, 146–151.
- (5) Palella, F. J.; Delaney, K. M.; Moorman, A. C.; Loveless, M. O.; Fuhrer, J.; Satten, G. A.; Aschman, D. J.; Holmberg, S. D.; The HIV Outpatient Study Investigators. Declining morbidity and mortality among patients with advanced human immunodeficiency virus infection. *N. Engl. J. Med.* **1998**, *338*, 853–860.
- (6) Israelski, D. M.; Remington, J. S. Toxoplasmosis in the non-AIDS immunocompromised host. *Curr. Clin. Top. Infect. Dis.* **1993**, *13*, 322–356.
- (7) Arantes, T. E.; Silveira, C.; Holland, G. N.; Muccioli, C.; Yu, F.; Jones, J. L.; Goldhardt, R.; Lewis, K. G.; Belfort, R., Jr. Ocular involvement following postnatally acquired *Toxoplasma gondii* infection in southern Brazil: A 28-year experience. *Am. J. Ophthalmol.* **2015**, *159*, 1002.
- (8) Jacobson, J. M.; Davidian, M.; Rainey, P. M.; Hafner, R.; Raasch, R. H.; Luft, B. J. Pyrimethamine pharmacokinetics in human immunodeficiency virus-positive patients seropositive for *Toxoplasma gondii*. *Antimicrob. Agents Chemother.* **1996**, *40*, 1360–1365.
- (9) McCabe, R. E. Antitoxoplasma chemotherapy. In *Toxoplasmosis: a Comprehensive Clinical Guide*; Joynson, D. H. M., Wreggitt, T. G., Eds.; Cambridge Univ. Press: Cambridge, 2001; pp 319–359.
- (10) Weiss, L. M.; Kim, K. Bradyzoite development. In *Toxoplasma gondii the Model Apicomplexan: Perspectives and Methods*; Weiss, L. M., Kim, K., Eds.; Academic Press: New York, 2007; pp 341–366.
- (11) Watts, E.; Zhao, Y.; Dhara, A.; Eller, B.; Patwardhan, A.; Sinai, A. P. Novel approaches reveal that *Toxoplasma gondii* bradyzoites within tissue cysts are dynamic and replicating entities *in vivo*. *mBio* **2015**, *6*, e01155-15.
- (12) Lourido, S.; Shuman, J.; Zhang, C.; Shokat, K. M.; Hui, R.; Sibley, L. D. Calcium-dependent protein kinase 1 is an essential regulator of exocytosis in *Toxoplasma*. *Nature* **2010**, *465*, 359–362.
- (13) Ojo, K. K.; Larson, E. T.; Keyloun, K. R.; Castaneda, L. J.; DeRocher, A. E.; Inampudi, K. K.; Kim, J. E.; Arakaki, T. L.; Murphy, R. C.; Zhang, L.; Napuli, A. J.; Maly, D. J.; Verlinde, C. L. M. J.; Buckner, F. S.; Parsons, M.; Hol, W. G. J.; Merritt, E. A.; Van Voorhis, C. *Toxoplasma gondii* calcium-dependent protein kinase 1 is a target for selective kinase inhibitors. *Nat. Struct. Mol. Biol.* **2010**, *17*, 602–607.
- (14) Wernimont, A. K.; Artz, J. D.; Finerty, P.; Lin, Y.; Amani, M.; Allali-Hassani, A.; senisterra, G.; Vedadi, M.; Tempel, W.; Mackenzie, F.; Chau, I.; Lourido, S.; Sibley, L. D.; Hui, R. Structures of apicomplexan calcium-dependent protein kinases reveal mechanism of activation by calcium. *Nat. Struct. Mol. Biol.* **2010**, *17*, 596–601.
- (15) Manning, G.; Whyte, D. B.; Martinez, R.; Hunter, T.; Sudarsanam, S. The protein kinase complement of the human genome. *Science* **2002**, *298*, 1912–1934.
- (16) Hui, R.; El Bakkouri, M.; Sibley, L. D. Designing selective inhibitors for calcium-dependent protein kinases in apicomplexans. *Trends Pharmacol. Sci.* **2015**, *36*, 452–460.
- (17) Bishop, A. C.; Shah, K.; Liu, Y.; Witucki, L.; Kung, C.; Shokat, K. M. Design of allele-specific inhibitors to probe protein kinase signaling. *Curr. Biol.* **1998**, *8*, 257–266.
- (18) Liu, Y.; Bishop, A.; Witucki, L.; Kraybill, B.; Shimizu, E.; Tsien, J.; Ubersax, J.; Blethrow, J.; Morgan, D. O.; Shokat, K. M. Structural basis for selective inhibition of Src family kinases by PP1. *Chem. Biol.* **1999**, *6*, 671–678.

- (19) Johnson, S. M.; Murphy, R. C.; Geiger, J. A.; DeRocher, A. E.; Zhang, Z.; Ojo, K. K.; Larson, E. T.; Perera, B. G.; Dale, E. J.; He, P.; Reid, M. C.; Fox, A. M.; Mueller, N. R.; Merritt, E. A.; Fan, E.; Parsons, M.; Van Voorhis, W. C.; Maly, D. J. Development of *Toxoplasma gondii* calcium-dependent protein kinase 1 (TgCDPK1) inhibitors with potent anti-toxoplasma activity. *J. Med. Chem.* **2012**, *55*, 2416–2426.
- (20) Larson, E. T.; Ojo, K. K.; Murphy, R. C.; Johnson, S. M.; Zhang, Z.; Kim, J. E.; Leiby, D. J.; Fox, A. M.; Reid, M. C.; Dale, E. J.; Perera, B. G.; Kim, J.; Hewitt, S. N.; Hol, W. G.; Verlinde, C. L.; Fan, E.; Van Voorhis, W. C.; Maly, D. J.; Merritt, E. A. Multiple determinants for selective inhibition of apicomplexan calcium-dependent protein kinase CDPK1. *J. Med. Chem.* **2012**, *55*, 2803–2810.
- (21) Murphy, R. C.; Ojo, K. K.; Larson, E. T.; Castellanos-Gonzalez, A.; Perera, B. G.; Keyloun, K. R.; Kim, J. E.; Bhandari, J. G.; Muller, N. R.; Verlinde, C. L.; White, A. C.; Merritt, E. A.; Van Voorhis, W. C.; Maly, D. J. Discovery of potent and selective inhibitors of calcium-dependent protein kinase 1 (CDPK1) from *Cryptosporidium parvum* and *Toxoplasma gondii*. *ACS Med. Chem. Lett.* **2010**, *1*, 331–335.
- (22) Doggett, J. S.; Ojo, K. K.; Fan, E.; Maly, D. J.; Van Voorhis, W. C. Bumped kinase inhibitor 1294 treats established *Toxoplasma gondii* infection. *Antimicrob. Agents Chemother.* **2014**, *58*, 3547–3549.
- (23) Lourido, S.; Zhang, C.; Lopez, M. S.; Tang, K.; Barks, J.; Wang, Q.; Wildman, S. A.; Shokat, K. M.; Sibley, L. D. Optimizing small molecule inhibitors of calcium-dependent protein kinase 1 to prevent infection by *Toxoplasma gondii*. *J. Med. Chem.* **2013**, *56*, 3068–3077.
- (24) Vidadala, R. S.; Rivas, K. L.; Ojo, K. K.; Hulverson, M. A.; Zambriski, J. A.; Bruzual, I.; Schultz, T. L.; Huang, W.; Zhang, Z.; Scheele, S.; DeRocher, A. E.; Choi, R.; Barrett, L. K.; Siddaramaiah, L. K.; Hol, W. G.; Fan, E.; Merritt, E. A.; Parsons, M.; Freiberg, G.; Marsh, K.; Kempf, D. J.; Carruthers, V. B.; Isoherranan, N.; Doggett, J. S.; Van Voorhis, W. C.; Maly, D. J. Development of an orally available and central nervous system (CNS) penetrant *Toxoplasma gondii* calcium-dependent protein kinase 1 (TgCDPK1) inhibitor with minimal human ether-a-go-go-related gene (hERG) activity for the treatment of toxoplasmosis. *J. Med. Chem.* **2016**, *59*, 6531–6546.
- (25) Hanefeld, U.; Rees, C. W.; White, A. J. P.; Williams, D. J. One-pot synthesis of tetrasubstituted pyrazoles - proof of regiochemistry. *J. Chem. Soc., Perkin Trans. 1* **1996**, *0*, 1545–1552.
- (26) Schenone, S.; Radi, M.; Musumeci, F.; Brullo, C.; Botta, M. Biologically driven synthesis of pyrazolo[3,4-d]pyrimidines as protein kinase inhibitors: an old scaffold as a new tool for medicinal chemistry and chemical biology studies. *Chem. Rev.* **2014**, *114*, 7189–7238.
- (27) Kwong, F. Y.; Buchwald, S. L. A general, efficient, and inexpensive catalyst system for the coupling of aryl iodides and thiols. *Org. Lett.* **2002**, *4*, 3517–3520.
- (28) Ley, S. V.; Thomas, A. W. Modern synthetic methods for copper-mediated C(aryl)-O, C(aryl)-N, and C(aryl)-S bond formation. *Angew. Chem., Int. Ed.* **2003**, *42*, 5400–5449.
- (29) Ma, D.; Cai, Q. N,N-dimethyl glycine-promoted ullmann coupling reaction of phenols and aryl halides. *Org. Lett.* **2003**, *5*, 3799–3802.
- (30) Prim, D.; Campagne, J.-m.; Andrioletti, B.; Joseph, D. Palladium-catalysed reactions of aryl halides with soft, non-organometallic nucleophiles. *Tetrahedron* **2002**, *58*, 2041–2075.
- (31) Zaretzki, J.; Matlock, M.; Swamidass, S. J. XenoSite: accurately predicting CYP-mediated sites of metabolism with neural networks. *J. Chem. Inf. Model.* **2013**, *53*, 3373–3383.
- (32) Bohm, H. J.; Banner, D.; Bendels, S.; Kansy, M.; Kuhn, B.; Muller, K.; Obst-Sander, U.; Stahl, M. Fluorine in medicinal chemistry. *ChemBioChem* **2004**, *5*, 637–643.
- (33) Barnes-Seeman, D.; Jain, M.; Bell, L.; Ferreira, S.; Cohen, S.; Chen, X. H.; Amin, J.; Snodgrass, B.; Hatsis, P. Metabolically stable tert-butyl replacement. *ACS Med. Chem. Lett.* **2013**, *4*, 514–516.
- (34) Hicken, E. J.; Marmsater, F. P.; Munson, M. C.; Schlachter, S. T.; Robinson, J. E.; Allen, S.; Burgess, L. E.; Delisle, R. K.; Rizzi, J. P.; Topalov, G. T.; Zhao, Q.; Hicks, J. M.; Kallan, N. C.; Tarlton, E.; Allen, A.; Callejo, M.; Cox, A.; Rana, S.; Klopfenstein, N.; Woessner, R.; Lyssikatos, J. P. Discovery of a novel class of imidazo[1,2-a]pyridines with potent PDGFR activity and oral bioavailability. *ACS Med. Chem. Lett.* **2014**, *5*, 78–83.
- (35) Shim, H. J.; Kim, H. I.; Lee, S. T. The associated pyrazolopyrimidines PP1 and PP2 inhibit protein tyrosine kinase 6 activity and suppress breast cancer cell proliferation. *Oncol. Lett.* **2017**, *13*, 1463–1469.
- (36) Lourido, S.; Jeschke, G. R.; Turk, B. E.; Sibley, L. D. Exploiting the unique ATP-binding pocket of toxoplasma calcium-dependent protein kinase 1 to identify its substrates. *ACS Chem. Biol.* **2013**, *8*, 1155–1162.
- (37) Yap, G. S.; Sher, A. Effector cells of both nonhemopoietic and hemopoietic origin are required for interferon (IFN)-gamma- and tumor necrosis factor (TNF)-alpha- dependent host resistance to the intracellular pathogen. *J. Exp. Med.* **1999**, *189*, 1083–1091.
- (38) Dunay, I. R.; Heimesaat, M. M.; Bushrab, F. N.; Muller, R. H.; Stocker, H.; Arasteh, K.; Kurowski, M.; Fitzner, R.; Borner, K.; Liesenfeld, O. Atovaquone maintenance therapy prevents reactivation of toxopasmic encephalitis in the murine model of reactivated toxoplasmosis. *Antimicrob. Agents Chemother.* **2004**, *48*, 4848–4854.
- (39) Zhang, C.; Lopez, M. S.; Dar, A. C.; Ladow, E.; Finkbeiner, S.; Yun, C. H.; Eck, M. J.; Shokat, K. M. Structure-guided inhibitor design expands the scope of analog-sensitive kinase technology. *ACS Chem. Biol.* **2013**, *8*, 1931–1938.
- (40) Long, A. M.; Zhao, H.; Huang, X. Structural basis for the potent and selective inhibition of casein kinase 1 epsilon. *J. Med. Chem.* **2012**, *55*, 10307–10311.
- (41) Dunay, I. R.; Chan, W. C.; Haynes, R. K.; Sibley, L. D. Artemisone and artemiside control acute and reactivated toxoplasmosis in the murine model. *Antimicrob. Agents Chemother.* **2009**, *53*, 4450–4456.
- (42) Minor, W.; Cymborowski, M.; Otwinowski, Z.; Chruszcz, M. HKL-3000: the integration of data reduction and structure solution—from diffraction images to an initial model in minutes. *Acta Crystallogr., Sect. D: Biol. Crystallogr.* **2006**, *62*, 859–866.
- (43) Bricogne, G.; Blanc, E.; Brandl, M.; Flensburg, C.; Keller, P.; W, P.; Roversi, P.; Sharff, A.; Smart, O. S.; Vonrhein, C.; Womack, T. O. BUSTER version 2.10.0. Global Phasing Ltd, Cambridge, United Kingdom. 2011.
- (44) Murshudov, G. N.; Vagin, A. A.; Dodson, E. J. Refinement of macromolecular structures by the maximum-likelihood method. *Acta Crystallogr., Sect. D: Biol. Crystallogr.* **1997**, *53*, 240–255.
- (45) Emsley, P.; Cowtan, K. Coot: model-building tools for molecular graphics. *Acta Crystallogr., Sect. D: Biol. Crystallogr.* **2004**, *60*, 2126–2132.
- (46) Davis, I. W.; Leaver-Fay, A.; Chen, V. B.; Block, J. N.; Kapral, G. J.; Wang, X.; Murray, L. W.; Arendall, W. B., 3rd; Snoeyink, J.; Richardson, J. S.; Richardson, D. C. MolProbity: all-atom contacts and structure validation for proteins and nucleic acids. *Nucleic Acids Res.* **2007**, *35*, W375–383.
- (47) Molecular Operating Environment (MOE), 2013.08. Chemical Computing Group ULC: Montreal, QC, Canada, 2017.
- (48) Fox, B. A.; Falla, A.; Rommereim, L. M.; Tomita, T.; Gigley, J. P.; Mercier, C.; Cesbron-Delauw, M. F.; Weiss, L. M.; Bzik, D. J. Type II *Toxoplasma gondii* KU80 knockout strains enable functional analysis of genes required for cyst development and latent infection. *Eukaryotic Cell* **2011**, *10*, 1193–1206.
- (49) Tobin, C. M.; Knoll, L. J. A patatin-like protein protects *Toxoplasma gondii* from degradation in a nitric oxide-dependent manner. *Infect. Immun.* **2012**, *80*, 55–61.
- (50) Wang, Z. T.; Harmon, S.; O’Malley, K. L.; Sibley, L. D. Reassessment of the role of aromatic amino acid hydroxylases and the effect of infection by *Toxoplasma gondii* on host dopamine. *Infect. Immun.* **2015**, *83*, 1039–1047.
- (51) Eid, S.; Turk, S.; Volkamer, A.; Rippmann, F.; Fulle, S. KinMap: a web-based tool for interactive navigation through human genome data. *BMC Bioinf.* **2017**, *18*, 16.